

Scensory: Real-Time Robotic Olfactory Perception for Joint Identification and Source Localization

Yanbaihui Liu¹, Erica Babusci¹, Claudia K. Gunsch¹, Boyuan Chen¹

<https://generalroboticslab.com/Scensory>

Abstract—While robotic perception has advanced rapidly in vision and touch, enabling robots to reason about indoor fungal contamination from weak, diffusion-dominated chemical signals remains an open challenge. We introduce *Scensory*, a learning-based robotic olfaction framework that simultaneously identifies fungal species and localizes their source from short time series measured by affordable, cross-sensitive VOC sensor arrays. Temporal VOC dynamics encode both chemical and spatial signatures, which we decode through neural networks trained on robot-automated data collection with spatial supervision. Across five fungal species, *Scensory* achieves up to 89.85% species accuracy and 87.31% source localization accuracy under ambient conditions with 3–7s sensor inputs. These results demonstrate real-time, spatially grounded perception from diffusion-dominated chemical signals, enabling scalable and low-cost source localization for robotic indoor environmental monitoring.

I. INTRODUCTION

Robotic perception has achieved extraordinary progress in vision, audition, and tactile sensing, enabling real-time object detection, mapping, and interaction in complex environments [1–6]. Despite these advances, robotic perception still remains limited in the chemical and microbial domains. Unlike light or sound, airborne chemical signals are low concentration, highly diffusive, temporally delayed, and often lack stable spatial gradients under indoor ambient conditions. These characteristics challenge standard robotic inference pipelines that rely on geometric structure, directional cues, or high signal-to-noise sensing. As a result, enabling robots to reason over weak, diffusion-dominated chemical signals remains an open challenge in robotic perception.

A representative and societally important testbed for studying diffusion-dominated chemical perception is indoor fungal contamination. Fungal growth poses significant risks to human health and building safety [7, 8], with airborne fungal emissions linked to asthma, allergies, and respiratory illness [9, 10]. Yet fungi and other microbial agents cannot be reliably detected through geometric, acoustic, or tactile cues until contamination becomes severe, making indoor fungal monitoring a compelling testbed for advancing robotic perception beyond geometry-driven modalities.

Traditional fungal detection methods, including culturing and molecular diagnostics such as qPCR and ITS sequencing [11, 12], provide high specificity but require laboratory infrastructure, sampling, or long processing times. These methods are not compatible with real-time, in-situ robotic deployment.

^{*}This work is supported by NSF Engineering Research Center for Precision Microbiome Engineering (PreMiEr) under award 2133504. ¹ All authors are from Duke University.

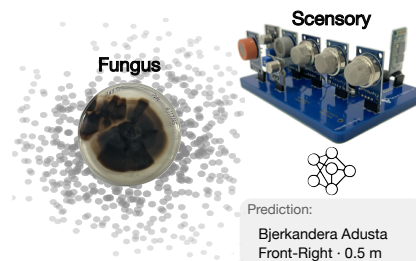


Fig. 1: **Scensory** infers fungal identity and source direction from passive volatile organic compound measurements, enabling robotic olfactory localization in real environments.

Electronic nose (eNose) systems [13] leverage volatile organic compounds (VOCs) released during fungal metabolism, such as alcohols, ketones, and sulfur-containing compounds, as discriminative chemical fingerprints [14–16]. When integrated with learning-based classifiers, these systems enable non-invasive fungal detection. Nevertheless, existing eNose systems primarily treat chemical perception as a static classification task. They typically operate in sealed environments to preconcentrate and do not address spatial inference, or robotic deployment in diffusion-dominated indoor spaces [17, 18].

In parallel, robotic odor source localization (OSL) has explored plume tracking and gradient-following strategies [19, 20]. These approaches rely on strong concentration gradients and structured airflow [21], assumptions that often break down in the home environment, where gradients are weak and unstable in most cases. Moreover, OSL methods typically target homogeneous gas sources rather than complex biological VOC mixtures.

Together, these limitations reveal a fundamental gap in robotics, as the ability for robots to jointly reason about “what” and “where” from weak ambient chemical signals remains largely unexplored. Bridging this gap requires moving beyond gradient-following heuristics or static classification toward spatiotemporal representation learning over diffusion-dominated dynamics.

We present *Scensory*, a robot-enabled olfactory perception system that performs simultaneous species identification and source localization using affordable cross-sensitive VOC arrays and deep learning. Coupled with our sensory array, we develop a spatiotemporal learning framework that decodes semantic and spatial information from diffusion-dominated VOC dynamics without relying on airflow modeling or strong concentration gradients. We evaluate *Scensory* in both passive multi-array configuration for environmental monitor-

ing, and a mobile single-array configuration for real-world deployments where only limited resources are available, or rapid, mobile, and cost-effective solutions are required.

Across 5 fungal species, Scensory achieves up to 89.85% species classification accuracy and 87.31% coarse source localization accuracy in the multi-array setting, and further enables single-array inference of species, direction, and distance. These results demonstrate that spatiotemporal learning over cross-sensitive chemical arrays can provide a promising solution to enable reliable joint semantic and spatial inference under weak diffusion.

II. RELATED WORK

A. Electronic Nose Systems and VOC Profiling

Electronic nose (eNose) systems employ cross-sensitive sensor arrays to encode volatile mixtures as high-dimensional response patterns, which are interpreted using statistical or deep learning models [13]. By leveraging the collective response of partially selective sensors, these systems can distinguish complex chemical mixtures without requiring highly specific sensing elements.

Recent advances demonstrate fungal discrimination in food, agricultural, and environmental applications [22–25], with ML-enhanced eNoses achieving high species-level performance in controlled settings [26, 27]. Advances in sensing technology also include biomimetic and bioinspired systems that improve robustness and multi-species recognition [28].

Despite semantic performance, most eNose systems treat chemical sensing as a classification problem under controlled conditions and do not incorporate spatial reasoning or robotic embodiment. Consequently, chemical identity is inferred without explicit reasoning about the physical origin of emissions under ambient diffusion.

B. Robotic Chemical Source Localization

Robotic chemical source localization (CSL) investigates how mobile agents can infer the spatial origin of airborne chemicals using onboard sensing and control. Classical formulations rely on plume tracking, gradient-following, or probabilistic search strategies [29, 30], typically evaluated under structured airflow or detectable concentration gradients. Beyond these gradient-based paradigms, recent work incorporates probabilistic reasoning and learning-based policies to improve robustness under dynamic and uncertain conditions [31]. These approaches generally assume a relatively homogeneous gas source and rely on measurable concentration structure to guide navigation.

To enhance search efficiency, several studies integrate visual scene understanding with chemical sensing. For example, semantic-based gas source localization combines object recognition with gas classification to constrain candidate source regions [32]. More recently, multimodal fusion frameworks integrate visual embeddings with olfactory signals to improve semantic reasoning about gas-emitting objects [33, 34]. These methods demonstrate the benefits of cross-modal cues for gas-related tasks, particularly when the emitting object is visually identifiable.

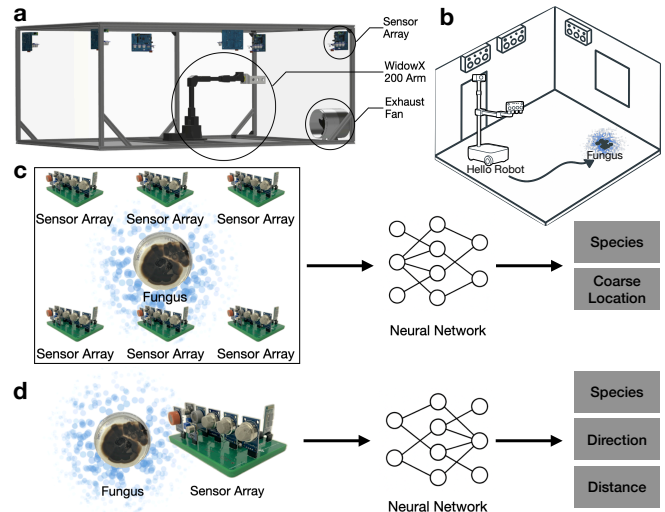


Fig. 2: System overview and sensing configurations of Scensory. (a) Robot-assisted data collection platform with spatially distributed VOC sensor arrays and robotic arm supervision. (b) Deployment modes: mobile robot with onboard sensor for mobile localization and fixed wall-mounted arrays for distributed monitoring. (c) Multi-array configuration for joint species identification and coarse source localization. (d) Single-array mobile configuration inferring species identity, direction, and distance from temporal VOC dynamics. Blue shading illustrates VOC diffusion.

However, most CSL formulations assume distinct gas types or visually identifiable emission sources. These assumptions become fragile in low-concentration indoor diffusion, where gradients are weak, unstable, and temporally entangled. Localizing such sources requires reasoning over subtle temporal chemical dynamics rather than relying on strong gradients or explicit visual anchors.

III. METHOD

A. System Overview

Scensory is a robotic olfactory perception framework that leverages VOC sensing and machine learning to infer fungal species identity and source location under ambient indoor conditions. The system integrates cross-sensitive VOC sensor arrays, robot-enabled spatial supervision, and learning-based inference within a unified pipeline.

Our framework supports two sensing configurations (Fig. 2). In the multi-array configuration, six spatially distributed sensor arrays concurrently capture VOC signals to jointly infer fungal identity and source location (Fig. 2c). In the single-array configuration, VOC time series from each individual array are processed independently, and spatial annotations are transformed into the local reference frame of each sensor to simulate mobile deployment (Fig. 2d). In this setting, spatial information must be inferred solely from temporal VOC dynamics using a single array. This dual-mode formulation enables us to evaluate both distributed monitoring and mobility-constrained localization under a shared data acquisition protocol.

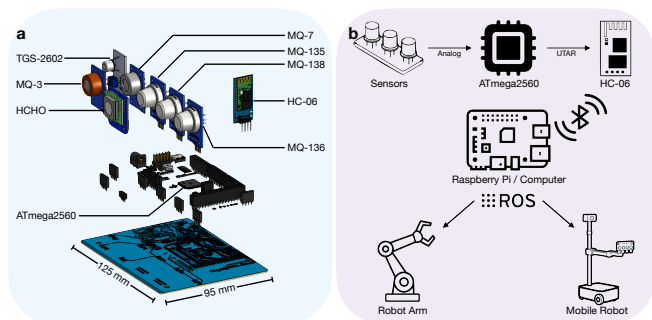


Fig. 3: Hardware setup and wireless communication pipeline. (a) Custom dual-layer PCB VOC sensor array (95×124 mm) integrating cross-sensitive gas sensors, environmental sensing, embedded microcontroller, and Bluetooth communication. (b) Digitized sensor signals are transmitted wirelessly to a Raspberry Pi 5 running ROS for synchronized data logging and robot coordination.

B. Robotic Sensing Framework

The VOC sensing system is built around a custom multi-sensor array (Fig. 3a) integrating six commercially available metal-oxide (MOx) gas sensors (MQ-3, MQ-7, MQ-135, MQ-136, MQ-138, and TGS2602), an electrochemical formaldehyde sensor (HCHO), and an SHT31 temperature-humidity sensor. These sensors are delicately selected for partially overlapping response profiles to alcohols, sulfur compounds, carbon monoxide, and other fungal metabolites.

Although individual MOx sensors are cross-sensitive and low-resolution, our key observation is that the combined multi-channel responses produce high-dimensional VOC activation patterns that vary across fungal species and spatial configurations. This configuration is conceptually analogous to RGB encoding in color representations, where overlapping responses from different sensors form a “chemical color” signature from each VOC mixture.

Sensing components are mounted on a 95×124 mm FR-4 printed circuit board (PCB) with shared firmware and calibration protocols. Analog outputs are digitized by an onboard ATmega2560 microcontroller and transmitted wirelessly via an HC-06 Bluetooth module to a Raspberry Pi 5 running ROS (Fig. 3b). Sensor packets are logged at 10 Hz and timestamp-aligned with robot control commands to ensure consistent temporal synchronization during data acquisition.

All learning-based experiments were conducted in a sealed acrylic testbed sized $1.5 \text{ m} \times 1.0 \text{ m} \times 0.6 \text{ m}$ and equipped with a side-mounted exhaust fan to ensure repeatable ambient conditions. A predefined spatial sampling protocol was implemented using a WidowX 200 robotic arm, which positioned fungal samples at various discrete waypoints within the testbed. At each waypoint, the arm paused for 10–20 s while sensor arrays recorded VOC dynamics.

C. Samples Preparation

We study five phylogenetically diverse fungal species, including *Xylaria cubensis.510* (*X.510*), *Penicillium toxicarium* (*P. toxicarium*), *Penicillium.513* (*P.513*), *Trichoderma.508*

(*T.508*), and *Bjerkandera adusta* (*B. adusta*). *B. adusta* and *P. toxicarium* were isolated from a test bed home’s basement via sterile swabbing and plating on PDA, while the rest were obtained from creosote-contaminated soil and associated roots. All fungal isolates were grown on Potato Dextrose Agar (PDA) under standardized conditions. Colonies were purified by repeated subculturing, and species were identified by ITS amplification and Sanger sequencing, with identity confirmed by comparison to NCBI reference sequences.

D. Data Acquisition and Processing

Sensor measurements and robot trajectories were recorded in ROS and aligned at 100 ms resolution to ensure temporal pairing between VOC signals and spatial annotations.

In the multi-array configuration, six statically distributed arrays recorded signals concurrently. Global source coordinates were obtained from robot kinematics, and directional quadrant labels were defined by dividing the x - y plane into four bins relative to each sensor array. Source distance was computed as the Euclidean distance between the array center and the robot end-effector.

For the single-array configuration, VOC streams were treated independently. Global source coordinates were transformed into the local reference frame of each sensor array to produce local quadrant labels and source distances for mobile deployment.

Data windows with source angles within 10° of quadrant boundaries were excluded to reduce ambiguity due to diffusion. For the single-array setting, windows were further retained only if the robot pose remained stable (variation < 5 cm over ≥ 7 s) and the source-to-array distance was between 0.1 m and 0.65 m.

MOx channels were smoothed using moving average and Savitzky–Golay filters, followed by baseline correction. Processed signals were segmented into 3 s windows. Multi-array inputs were constructed by concatenating synchronized readings from all six arrays, while single-array inputs were processed independently after local transformation. All channels were standardized using z-score normalization, and random oversampling was applied to address class imbalance.

Training and validation sets were formed by a 70/30 split within the same collection dataset. We further evaluated on a held-out test set of comparable size collected on different days using independent fungal culture batches, with no overlap in collection sessions between train/val and test.

E. Model Architecture

Sensory uses a family of task-specific models that follow a common architectural template, as shown in Fig. 4. The template defines a consistent structure, while model parameters are not shared. Given the limited data per task, we train each task-specific model independently rather than with joint multi-task optimization.

The template is applied in both sensing configurations introduced in Sec. III-A. Multi-array input is the synchronized joint stream from all six arrays, while single-array input is one array’s time series expressed in its local frame. Each

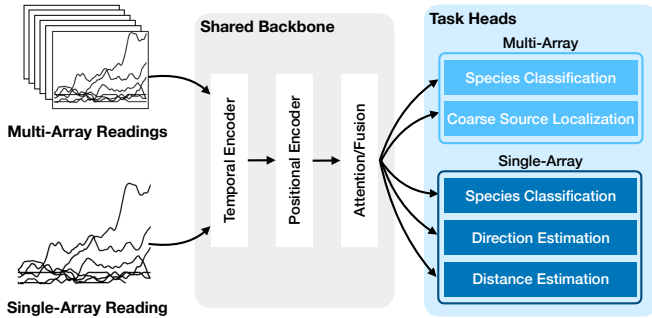


Fig. 4: Sensory model. The model takes time series data as input, extracts spatiotemporal features, and outputs predicted species, direction, or distance of the contamination.

model follows temporal encoding, positional encoding, and temporal aggregation flow to produce a fixed-dimensional embedding for the task-specific head.

We apply this template to five different tasks. In the multi-array setting, we train separate models for species classification and coarse source localization. In the single-array setting, we train separate models for species classification, direction estimation in the array’s local frame, and distance estimation.

Temporal modeling is critical because MOx sensors exhibit slow rise and recovery dynamics under diffusion-dominated conditions. Features in weak indoor diffusion emerge from temporal response patterns rather than instantaneous concentration values. Each model therefore begins with a temporal encoder tailored to the dominant temporal structure of its task. For species classification in either configuration, we use a temporal convolutional network with dilated causal convolutions and residual connections to capture local response dynamics. For single-array direction and distance, we use a bidirectional LSTM to model longer-range temporal dependencies. For multi-array coarse source localization, we use a multi-branch 1D CNN that encodes each array independently before fusing embeddings. This design preserves spatial separation across arrays while maintaining temporal modeling within each branch.

Then, we apply sinusoidal positional encoding to preserve temporal order before aggregation. Temporal aggregation is implemented with multi-head self-attention in the TCN- and LSTM-based models. In the multi-array coarse source localization task, aggregation is performed through a fusion module, while the distance estimation model applies an additional learned attention pooling before the final prediction. We use attention-based aggregation to capture relevant temporal features more effectively than simple mean pooling. All models use the same embedding dimensionality to maintain architectural consistency across tasks. No additional modalities are used beyond the preprocessed VOC and environmental channels described in Sec. III-B.

Each task head is implemented as a small MLP on top of the backbone embedding. The multi-array models predict species over five fungal classes and a coarse quadrant label over four directional bins. The single-array models predict species, a direction label in the array’s local frame, and a

TABLE I: Per-class performance under multi-array and single-array sensing configurations. P, R, and F1 denote class-wise precision, recall, and F1-score.

	Multi-Array Configuration			Single-Array Configuration		
	P(%)	R(%)	F1(%)	P(%)	R(%)	F1(%)
X. 510	77.13	80.82	78.74	73.67	67.25	70.18
P. toxicarium	84.91	80.64	82.26	77.35	68.93	72.87
P. 513	82.17	82.85	82.43	54.52	65.84	59.46
T. 508	90.06	81.93	85.52	62.49	67.83	64.58
B. adusta	84.31	92.14	87.97	70.63	70.17	70.03
Bin 0	87.85	84.96	86.27	33.94	46.18	39.07
Bin 1	92.06	85.42	88.53	36.64	50.97	42.65
Bin 2	90.43	83.19	86.53	64.52	46.61	54.19
Bin 3	64.91	82.73	72.63	57.23	67.93	62.13

scalar source distance. Classification models are trained with cross-entropy loss, and distance estimation model with mean squared error. Training protocol and preprocessing follow Sec. III-D.

IV. EXPERIMENT

A. Multi-array sensing

We first evaluate whether synchronized measurements from six spatially distributed sensor arrays provide sufficient spatiotemporal structure for joint semantic and spatial inference under ambient diffusion.

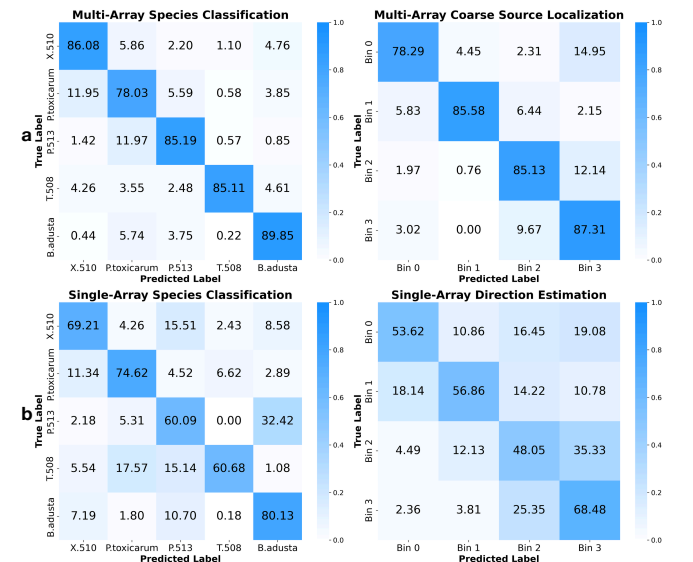


Fig. 5: Confusion matrices for species classification and spatial inference tasks, reported in percentage accuracy. **a**, Results for the multi-array configuration. **b**, Results for the single-array configuration. Left: species classification. Right: spatial prediction.

1) *Species classification*: The model achieves high accuracy across five fungal species, with class-wise recognition ranging from 78.03% to 89.85% as shown in (Fig. 5a-left). The highest classification accuracy was observed for *B. adusta* (89.85%). The lowest accuracy was observed for *P. toxicarium* (78.03%), which exhibited notable confusion with the related *P.513* isolate. The confusion matrix indicates that

most errors occur between phylogenetically related species, suggesting partially overlapping VOC signatures. Cross-genus confusion remains limited and does not dominate the error distribution.

To ensure statistical robustness, we evaluated the same test dataset using models with identical architecture and training methodology but different random seeds, then computed precision, recall, and F1-scores by averaging performance across these independent training runs. Performance was consistently strong across all metrics, with most species exceeding 0.8 in both precision and recall, showing balanced sensitivity and specificity (Table. I). These results indicate that distributed cross-sensitive arrays encode sufficient spatiotemporal structure for reliable multi-class identification under ambient conditions.

2) *Spatial localization*: We next evaluate coarse source localization by predicting one of four directional quadrants. Our model gives quadrant classification accuracy ranging from 78.29% to 87.31% across the spatial bins (Fig. 5a-right). The highest accuracy is achieved in Bin 3 (87.31%), while the lowest is in Bin 0 (78.29%)

Most errors occur between adjacent quadrants, consistent with the continuous nature of diffusion under indoor ambient conditions. Importantly, confusions with the opposite quadrant are rare, and the model does not collapse to predicting any single direction overall

Table I reports precision, recall, and F1-score per bin. While overall performance is stable across runs, Bin-level asymmetry is observed, suggesting that certain regions are more prone to false positives or false negatives. This does not imply a global directional bias, instead, it reflects quadrant-dependent precision–recall trade-offs that are not fully reflected by accuracy alone.

B. Single-array sensing

We next evaluate the more challenging single-array setting, where inference must rely solely on temporal VOC dynamics measured at a single sensing unit. This configuration corresponds to mobile or targeted deployment, where a fixed multi-array infrastructure is unavailable.

1) *Species classification*: Single-array species classification achieves class-wise accuracies ranging from 60.09% to 80.13% (Fig. 5b-left). Compared with the multi-array configuration, performance decreases as expected due to the loss of spatial redundancy. The confusion matrix shows that most errors are concentrated among chemically similar species, indicating that disambiguation becomes more difficult without distributed spatial measurements.

Precision, recall, and F1-score remain stable across five independent training runs (Table I), with class-wise precision and recall generally spanning 0.55 to 0.80. These results indicate that a single sensing unit still preserves sufficient temporal structure for effective species discrimination, even without spatial triangulation.

2) *Source direction estimation*: Directional inference using single-array measurements proved significantly more

challenging than multi-array spatial localization, with accuracies ranging from 48.08% to 68.65% across four spatial bins (Fig. 5b-right). Unlike multi-array systems that leverage simultaneous concentration gradients across multiple positions, single-array approaches must infer source direction from the subtle and slow temporal evolution of mixed chemical signals. This is further complicated by ambient airflow, variable diffusion rates across different species, and the overlapping response characteristics to complex chemical mixtures.

Bin-wise precision, recall, and F1-score are summarized in Table I. Bin 3 exhibits the highest overall performance with balanced precision and recall, and Bin 2 shows a conservative classification profile characterized by high precision but low recall. This spatial heterogeneity likely reflects position-dependent variations in airflow patterns and sensor sensitivity within the experimental layout. Nevertheless, all bins exceeded well beyond the 25% chance level, confirming the presence of usable spatial signal even under restricted sensor availabilities.

3) *Source distance estimation*: We further evaluated whether the single-array configuration could estimate the distance between the fungal source and the sensor array. This represents a novel capability for airborne fungal localization, since distance inference from short-temporal VOC patterns with a single sensor array has not been previously demonstrated. Across all species, the model achieved mean absolute error (MAE) between 0.1097 m and 0.1311 m (Tab. II). The lowest error was observed for *T.508* (MAE: 0.1097 m) and the highest for *P. toxicarium* (MAE: 0.1311 m).

To contextualize these errors relative to source size, we define a resolution ratio as the petri dish radius (0.045 m) divided by MAE:

$$\text{Resolution Ratio} = \frac{r_{\text{plate}}}{\text{MAE}}$$

A resolution ratio below one indicates that the average localization error is larger than the physical source size, and higher values correspond to better performance. Across species, resolution ratios ranged from 0.34 to 0.41 (Tab. II), indicating that the average localization error slightly exceeds the physical extent of the source. Although this accuracy is coarse, it remains sufficient for approximate robotic search, where the goal is to guide the platform into the vicinity of the contamination source rather than to recover point-level localization.

TABLE II: Distance estimation performance across fungal species. MAE and RMSE are reported in meters, MSE is reported in square meters. Resolution Ratio quantifies the relative spatial resolution (plate radius = 0.045 m).

Species	MAE [m]	MSE [m ²]	RMSE [m]	Resolution Ratio
<i>X.510</i>	0.1246	0.0239	0.1513	0.36
<i>P. toxicarium</i>	0.1311	0.0258	0.1601	0.34
<i>P.513</i>	0.1198	0.0198	0.1388	0.38
<i>T.508</i>	0.1097	0.0182	0.1358	0.41
<i>B. adusta</i>	0.1169	0.0217	0.1467	0.39

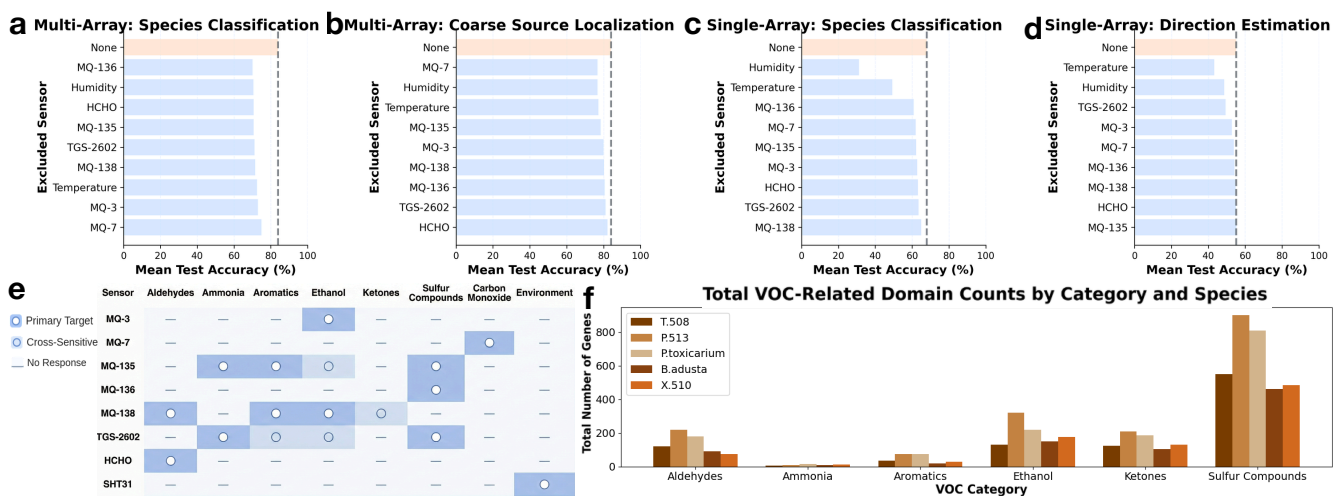


Fig. 6: Sensor ablation analysis. (a–d) Channel exclusion results for species classification and source localization tasks. Bars denote mean test accuracy over five runs; dashed lines indicate full-channel performance, and “None” corresponds to the full model. (e) Sensor response matrix across major VOC classes. (f) Total VOC-related InterPro domain counts by category and species, highlighting the prominence of sulfur-related pathways.

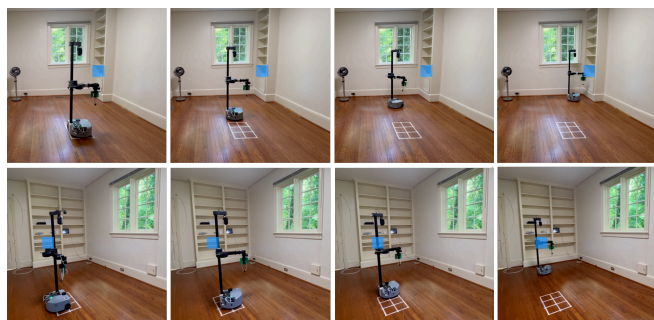


Fig. 7: Real-world Olfactory-Based Navigation. The blue square indicates where the fungal plates are placed.

C. Real World Experiment

We conducted a real-world qualitative experiment in a residential home to assess the potential to deploy our model in the open world. A mobile robot equipped with a single Scensory array continuously inferred species identity and source location from real-time VOC signals and navigated toward the predicted source (Fig. 7). Both trials were completed without environmental recalibration, indicating potential for practical indoor mold monitoring and source localization. Though this experiment shows promising qualitative results, robust deployment in the open world will require more data collection and coverage. We leave such study as future work.

D. Sensor channel ablation study

To better understand how our model learns to interpret the olfactory signals, we performed systematic ablation studies on both multi-array and single-array models (Fig. 6a–d) by removing each sensor channel in turn and logging the changes in the classification and localization accuracies from the original performance. This analysis provides a direct measure of sensor-channel importance and helps identify which modalities contribute most to semantic and

spatial inference. We further compare these patterns with InterPro-based pathway annotations to examine whether the learned importance ranking is consistent with known fungal metabolic signatures [35].

Our results show that environmental sensors exhibited higher importance in single-array configurations. For example, in single-array configurations, temperature and humidity sensors contributed an average of 27.79% to classification performance (18.72% for temperature, 36.85% for humidity), compared to 6.04% (5.09% for temperature, 6.98% for humidity) in the multi-array setting. Similarly, for localization performance, these sensors contributed 9.3% on average (12.01% for temperature, 6.59% for humidity) in the single-array mode, versus 7.02% (6.79% for temperature, 7.25% for humidity) in the multi-array configuration. This trend suggests that environmental context becomes more important when spatial redundancy is not available, since a single array must rely more heavily on temporal modulation of the local VOC signal.

Sulfur-sensitive sensors, including MQ-135, MQ-136, and TGS-2602, consistently rank among the most influential channels for species classification (Fig. 6a–e). This importance pattern is consistent with the InterPro analysis in Fig. 6f, where sulfur-metabolism-related domains are prevalent across the fungal isolates. While the ablation study is purely computational, the agreement between sensor importance and pathway annotations suggests that the learned model is capturing biologically meaningful signal structure.

E. Baseline Comparison

We chose to conduct baseline comparisons in the single-array setting because it represents the more challenging regime in our shared experimental template. The baselines include 1) a *Drosophila*-inspired denoise–aggregate–MLP pipeline [28], 2) a static-feature MLP using per-channel

mean, standard deviation, and maximum, and 3) a Random Forest trained on the same summary statistics. All methods use the same 3 s input window (30×9) and identical train/validation/test splits, so performance differences primarily reflect how temporal information is modeled.

As shown in Table III, Scensory achieves the best species performance with 69.94% accuracy and 68.97% F1-score, outperforming the static MLP (66.23%, 65.24%), Random Forest (59.83%, 58.73%), and the *Drosophila* baseline (36.67%, 37.75%). For directional bin prediction, Scensory reaches 57.00% accuracy and 52.48% F1-score. Although Random Forest attains slightly higher accuracy (58.31%), Scensory yields higher F1 and recall, indicating more balanced predictions across bins.

These results suggest that the task-specific temporal encoder with attention captures discriminative structure beyond what can be recovered from summary statistics or denoise-aggregate pipelines, particularly under weak and diffusion-dominated VOC conditions.

TABLE III: Single-array baseline comparison for species classification and spatial bin prediction.

Method	Task	Acc(%)	P(%)	R(%)	F1(%)
<i>Drosophila</i>	Species	36.67	38.65	40.32	37.75
	Directions	33.61	31.25	35.80	30.35
Static MLP	Species	66.23	66.70	66.28	65.24
	Directions	45.06	38.24	45.72	38.88
Random Forest	Species	59.83	61.62	61.03	58.73
	Directions	58.31	51.39	52.36	50.33
Scensory (ours)	Species	69.94	70.01	68.95	68.97
	Directions	57.00	50.49	56.75	52.48

V. CONCLUSIONS, LIMITATIONS, AND FUTURE WORK

We show that fungal species identification and source localization are feasible with cross-sensitive MOx arrays when combined with robot-automated data collection and spatiotemporal learning. Scensory runs in real time under ambient conditions without specialized enclosures or sample pre-concentration. Our qualitative deployments in a residential setting indicate its potential for transfer beyond the lab.

Our results show that temporal VOC responses encode both chemical identity and coarse source-localization cues, even under weak and heterogeneous indoor diffusion. Learning over short temporal windows enables joint species classification and source localization without relying on engineered airflow or explicit gradient estimation.

However, we also observe a clear performance drop in the single-array setting. This reflects the trade-off between mobility and spatial redundancy. Closely related species remain difficult to distinguish, and the current models assume a single dominant species per environment. Future work will target mixed-species inference, extension to more taxa and environments, and tighter integration of ablation-driven sensor selection with hardware design.

REFERENCES

[1] J. Redmon, S. Divvala, R. Girshick, and A. Farhadi, “You only look once: Unified, real-time object de-

tection,” in *Proceedings of the IEEE conference on computer vision and pattern recognition*, 2016, pp. 779–788.

[2] K. He, G. Gkioxari, P. Dollár, and R. Girshick, “Mask R-CNN,” in *Proceedings of the IEEE International Conference on Computer Vision (ICCV)*, 2017, pp. 2961–2969.

[3] A. Wang, H. Chen, L. Liu, K. Chen, Z. Lin, J. Han, and G. Ding, “YOLOv10: Real-time end-to-end object detection,” in *Advances in Neural Information Processing Systems*, vol. 37, 2024, arXiv:2405.14458.

[4] H. Su, F. Song, C. Ma, W. Wu, and J. Yan, “RoboSense: Large-scale dataset and benchmark for egocentric robot perception and navigation in crowded and unstructured environments,” in *Proceedings of the IEEE/CVF Conference on Computer Vision and Pattern Recognition (CVPR)*, 2025.

[5] J. Liu and B. Chen, “Sonicsense: Object perception from in-hand acoustic vibration,” in *Proceedings of The 8th Conference on Robot Learning*, vol. 270. PMLR, 2024, pp. 4332–4353.

[6] Y. Liu and B. Chen, “Wildfusion: Multimodal implicit 3d reconstructions in the wild,” in *Proceedings of the IEEE International Conference on Robotics and Automation (ICRA)*, 2025, arXiv:2409.19904.

[7] M. J. Mendell, A. G. Mirer, K. Cheung, M. Tong, and J. Douwes, “Respiratory and allergic health effects of dampness, mold, and dampness-related agents: a review of the epidemiologic evidence,” *Environmental health perspectives*, vol. 119, no. 6, pp. 748–756, 2011.

[8] S. Lee, S.-H. Ryu, W. J. Sul, S. Kim, D. Kim, and S. Seo, “Association of exposure to indoor molds and dampness with allergic diseases at water-damaged dwellings in korea,” *Scientific Reports*, vol. 14, no. 1, p. 135, 2024.

[9] C. Tischer, C.-M. Chen, and J. Heinrich, “Association between domestic mould and mould components, and asthma and allergy in children: a systematic review,” *European Respiratory Journal*, vol. 38, no. 4, pp. 812–824, 2011.

[10] D. Caillaud, B. Leynaert, M. Keirsbulck, and R. Nadif, “Indoor mould exposure, asthma and rhinitis: findings from systematic reviews and recent longitudinal studies,” *European Respiratory Review*, vol. 27, no. 148, 2018.

[11] M. Pitkäranta, T. Meklin, A. Hyvärinen, A. Nevalainen, L. Paulin, P. Auvinen, U. Lignell, and H. Rintala, “Molecular profiling of fungal communities in moisture damaged buildings before and after remediation—a comparison of culture-dependent and culture-independent methods,” *BMC microbiology*, vol. 11, pp. 1–16, 2011.

[12] C. L. Halliday, S. Kidd, T. C. Sorrell, and S. C. Chen, “Molecular diagnostic methods for invasive fungal disease: the horizon draws nearer?” *Pathology-Journal of the RCPA*, vol. 47, no. 3, pp. 257–269, 2015.

[13] K. Persaud and G. Dodd, “Analysis of discrimination mechanisms in the mammalian olfactory system using

- a model nose,” *Nature*, vol. 299, no. 5881, pp. 352–355, 1982.
- [14] P. Buzzini, C. Gasparetti, B. Turchetti, M. R. Cramarossa, A. Vaughan-Martini, A. Martini, U. M. Pagnoni, and L. Forti, “Production of volatile organic compounds (vocs) by yeasts isolated from the ascocarps of black (tuber melanosporum vitt.) and white (tuber magnatum pico) truffles,” *Archives of microbiology*, vol. 184, pp. 187–193, 2005.
- [15] H. Aisala, J. Sola, A. Hopia, K. M. Linderborg, and M. Sandell, “Odor-contributing volatile compounds of wild edible nordic mushrooms analyzed with hs-spmegc-ms and hs-spmegc-ofid,” *Food chemistry*, vol. 283, pp. 566–578, 2019.
- [16] S. Sommer, M. A. Fraatz, J. Büttner, A. A. Salem, M. Rühl, and H. Zorn, “Wild strawberry-like flavor produced by the fungus wolfiporia cocos—identification of character impact compounds by aroma dilution analysis after dynamic headspace extraction,” *Journal of Agricultural and Food Chemistry*, vol. 69, no. 47, pp. 14 222–14 230, 2021.
- [17] Y. Guo, W. Jud, F. Weigl, A. Ghirardo, R. R. Junker, A. Polle, J. P. Benz, K. Pritsch, J.-P. Schnitzler, and M. Rosenkranz, “Volatile organic compound patterns predict fungal trophic mode and lifestyle,” *Communications biology*, vol. 4, no. 1, p. 673, 2021.
- [18] K. Karlshøj, P. V. Nielsen, and T. O. Larsen, “Differentiation of closely related fungi by electronic nose analysis,” *Journal of Food Science*, vol. 72, no. 6, pp. M187–M192, 2007.
- [19] A. T. Hayes, A. Martinoli, and R. M. Goodman, “Distributed odor source localization,” *IEEE Sensors Journal*, vol. 2, no. 3, pp. 260–271, 2002.
- [20] A. Celani, E. Villermaux, and M. Vergassola, “Odor landscapes in turbulent environments,” *Physical Review X*, vol. 4, no. 4, p. 041015, 2014.
- [21] S. H. Singh, F. van Breugel, R. P. Rao, and B. W. Brunton, “Emergent behaviour and neural dynamics in artificial agents tracking odour plumes,” *Nature machine intelligence*, vol. 5, no. 1, pp. 58–70, 2023.
- [22] Y. Li, Z. Wang, T. Zhao, H. Li, J. Jiang, and J. Ye, “Electronic nose for the detection and discrimination of volatile organic compounds: Application, challenges, and perspectives,” *TrAC Trends in Analytical Chemistry*, p. 117958, 2024.
- [23] F. J. Cabañes, N. Sahgal, M. R. Bragulat, and N. Magan, “Early discrimination of fungal species responsible of ochratoxin a contamination of wine and other grape products using an electronic nose,” *Mycotoxin research*, vol. 25, pp. 187–192, 2009.
- [24] Q. Liu, N. Zhao, D. Zhou, Y. Sun, K. Sun, L. Pan, and K. Tu, “Discrimination and growth tracking of fungi contamination in peaches using electronic nose,” *Food Chemistry*, vol. 262, pp. 226–234, 2018.
- [25] Z. Suchorab, M. Frąć, Ł. Guz, K. Oszust, G. Łagód, A. Gryta, N. Bilińska-Wielgus, and J. Czerwiński, “A method for early detection and identification of fungal contamination of building materials using e-nose,” *PloS one*, vol. 14, no. 4, p. e0215179, 2019.
- [26] A. Makarichian, R. A. Chayjan, E. Ahmadi, S. S. Mohtasebi, and D. Zafari, “Use of e-nose in inspecting the effect of processing type on the aroma of garlic (allium sativum l.): a critical hint in the quality assessment,” *Food Production, Processing and Nutrition*, vol. 6, no. 1, p. 52, 2024.
- [27] P. Borowik, P. Pluta, M. Tkaczyk, A. Okorski, R. Tarakowski, and T. Oszako, “Detection of fusarium poae infestation in wheat grain by measurement with two electronic noses,” *Engineering Proceedings*, vol. 82, no. 1, 2024.
- [28] X. Yue, J. Wang, H. Yang, Z. Li, F. Zhao, W. Liu, P. Zhang, H. Chen, H. Jiang, N. Qin, *et al.*, “A drosophila-inspired intelligent olfactory biomimetic sensing system for gas recognition in complex environments,” *Microsystems & Nanoengineering*, vol. 10, no. 1, p. 153, 2024.
- [29] A. Loutfi, S. Coradeschi, A. J. Lilienthal, and J. Gonzalez, “Gas distribution mapping of multiple odour sources using a mobile robot,” *Robotica*, vol. 27, no. 2, pp. 311–319, 2009.
- [30] A. Marjovi and L. Marques, “Multi-robot odor distribution mapping in realistic time-variant conditions,” in *2014 IEEE International Conference on Robotics and Automation (ICRA)*, P. Editors, Ed. IEEE, 2014, pp. 3720–3727.
- [31] S. Hassan, L. Wang, and K. R. Mahmud, “Robotic odor source localization via vision and olfaction fusion navigation algorithm,” *Sensors*, vol. 24, no. 7, p. 2309, 2024.
- [32] J. Monroy, J.-R. Ruiz-Sarmiento, F.-A. Moreno, F. Melendez-Fernandez, C. Galindo, and J. Gonzalez-Jimenez, “A semantic-based gas source localization with a mobile robot combining vision and chemical sensing,” *Sensors*, vol. 18, no. 12, p. 4174, 2018.
- [33] L. Zhang, J. Shi, X. Wei, and L. Feng, “Oevs-fusion: Olfactory-enhanced visual semantic recognition framework for ground stain detection in indoor environments,” *Sensors and Actuators B: Chemical*, vol. 440, p. 137902, 2025.
- [34] E. Ozguroglu, J. Liang, R. Liu, M. Chiquier, M. De-Tienne, W. W. Qian, A. Horowitz, A. Owens, and C. Vondrick, “New york smells: A large multimodal dataset for olfaction,” *arXiv preprint arXiv:2511.20544*, 2025.
- [35] M. Blum, A. Andreeva, L. C. Florentino, S. R. Chuguransky, T. Grego, E. Hobbs, B. L. Pinto, A. Orr, T. Paysan-Lafosse, I. Ponamareva, *et al.*, “Interpro: the protein sequence classification resource in 2025,” *Nucleic acids research*, vol. 53, no. D1, pp. D444–D456, 2025.